8.1. Introduction

In this Chapter, the impact of dopants (Fe and Cr) on the performance of pure Zinc cobaltite has been analyzed by XRD, Raman, FESEM-EDAX, CV, GCD and EIS characterizations. Double dopants are used due to the fact the $ZnCoFe_2O_4$ reported in the literature (**Rani et al., 2018)** suffers from severe potential drop due to active mobility of dual ions and has got severe diffusion effects seen in the supercapacitive profile. Also, the photo electrochemical evaluation of Zinc chromate exhibited more probability of irreversible reduction of Chromium from Cr^{4+} to Cr^{3+} preventing the mechanism of Zn when they coexist. Hence opting of single dopant of either Fe or Cr is unfavourable. But to harvest the advantage of stability that these atoms would offer to the $ZnCo_2O_4$ is attempted since this has not been evaluated in the literature to the best of author's knowledge.

8.2. X-Ray Diffraction Analysis of Fe,Cr:$ZnCo_2O_4$

Figure 58 shows the X-ray diffractogram (XRD) along with Rietveld refinement analysis of Fe and Cr doped $ZnCo_2O_4$. The refined diffractogram of Fe, Cr: $ZnCo_2O_4$ exhibits the spinel cubic phase with the no secondary phases and impurities. Also, there is no change in the crystal lattice which is the evidence for the completed chemical reactions during the synthesis process, and all of the parent elements have been reduced to the desired product. The observed pattern coincides with the standard data (JCPDS Card No.: 23-1390) confirms the formation of spinel-cubic crystal lattice with $Fd\bar{3}m$ space group. According to standard JCPDS card 23-1390, all the diffraction peaks of the doped sample at 19.11˚, 31.3˚, 36.71˚, 38.5˚, 44.7˚, 59.4˚ and 65.2˚are marked with their corresponding miller planes (111), (220), (311), (222), (400), (511) and (440) respectively.

The obtained parameters from Rietveld refinement are given in Table 23. The refined parameters such as W_R=4.863 and GOF=1.60 validate the perfect fit of the experimental data with the theoretical data. The generated (hkl) values from the Rietveld analysis well matches with (hkl) values of standard JCPDS further reconfirming the spinel crystal structure of $ZnCo_2O_4$ while doping.

Atomic arrangements of Fe and Cr doped $ZnCo_2O_4$ obtained from the VESTA software is shown in Figure 59. In the crystal structure seen in Figure 59, oxygen atoms are located behind the Co atoms. Hence, the inset shows the crystal structure of Fe and Cr doped Zinc cobaltite without cobalt atom. From Figure 59, it is clear that the divalent cations of 'Zn' in tetrahedral sites are occupied by the Fe and Cr dopants. Hence, the atomic coordinate of Zn changes for doped Zinc cobaltite.

In Fe, Cr: $ZnCo_2O_4$ sample, the positional coordinates of Zn atoms (0.1250,0.1250,0.1250), Fe atoms (0.0078,0.0078,0.0078), Cr atoms (0.5702,0.5702,0.5702), Co atoms (0.6250, 0.6250, 0.6250) and O (0.377, 0.377, 0.377) is obtained after the Rietveld fit. The positional coordinates of Zinc have been changed from (0,0,0) to (0.1250,0.1250,0.1250) which is due to the incorporation of Fe and Cr in the pristine lattice. From the unit cell obtained by Rietveld and visualized using Vesta softwares, shows 5 atoms of Zn per unit cell, 6 atoms of Cr per unit cell, 4 atoms of Fe per unit cell, 8 atoms of Co per unit cell and 24 atoms of O per unit cell. Thus the double doping of $ZnCo_2O_4$ with Fe and Cr leaves out nearly 28% vacancy in Zn site with Co or O sites undisturbed.

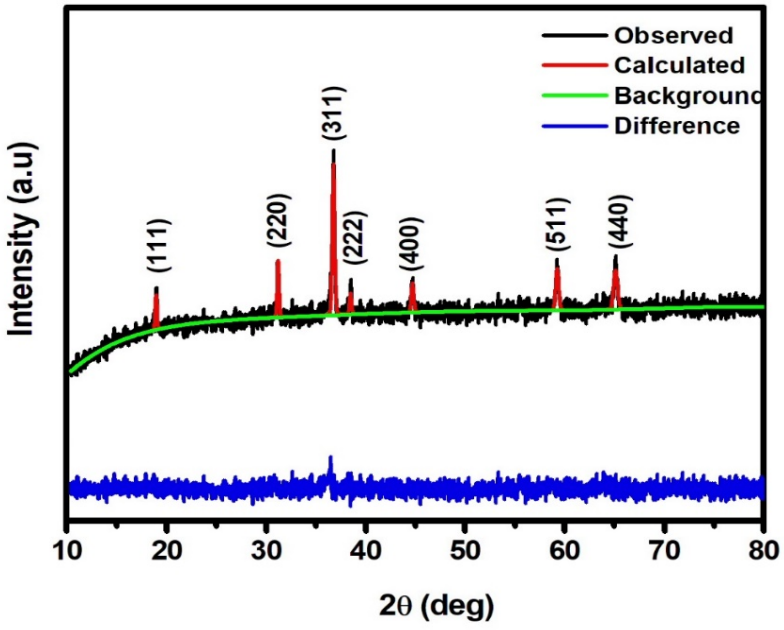

Figure 58 - Rietveld refined X-ray Diffractogram of Fe,Cr:$ZnCo_2O_4$

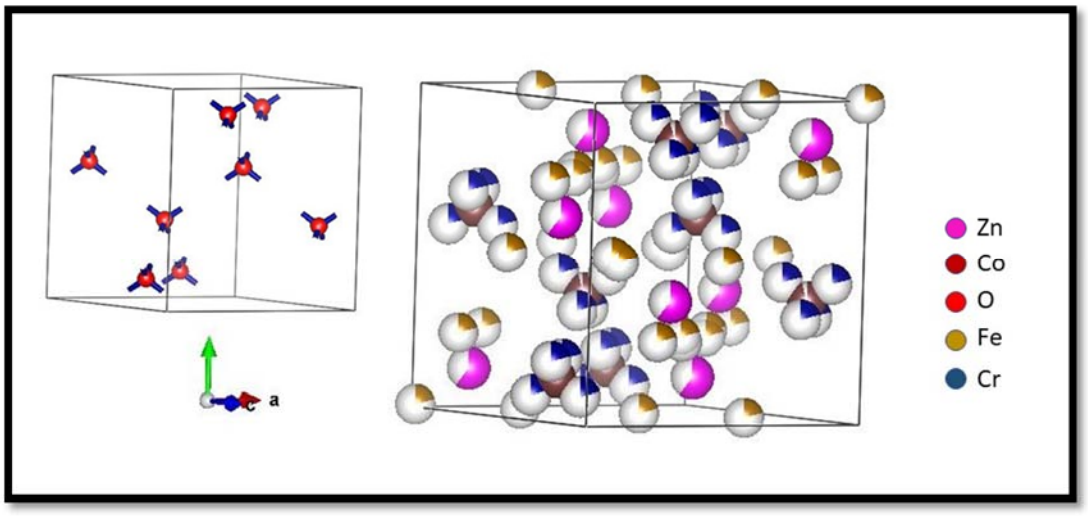

Figure 59 - Rietveld refined crystal structure of Fe,Cr:$ZnCo_2O_4$; inset shows the position of oxygen

The parameters calculated from the XRD analysis are shown in Table 24. The diffraction peaks are broadened due to the incorporation of Fe and Cr dopants into the $ZnCo_2O_4$ matrix. The FWHM (β) of high intense peak (311) plane for doped sample is increased and the obtained β value is 0.28°. The change in FWHM value decreases the crystallite size as per Scherrer's formula. On the other hand, d spacing ($d_{(311)}$) of Fe and Cr doped $ZnCo_2O_4$ is slightly varied compared to pristine $ZnCo_2O_4$. The corresponding $d_{(311)}$ value for Fe and Cr doped $ZnCo_2O_4$ is 2.44 Å.

The doped sample has the highest d spacing that possesses the lowest crystallite size value and the value is 27.63 nm. The doped sample has a lattice parameter value of 8.094 Å which is higher than the undoped Zinc cobaltite. Because, the ionic radii of the dopants (Fe^{3+} =0.69 Å and Cr^{3+}=0.61 Å) are high compared to the radius of Zn^{2+} (0.60 Å) which leads to change in the lattice constant resulting in expansion of the Zinc cobaltite lattice. The incorporation of bigger ions into smaller ion shows the higher strain value of 0.22 for doped sample which may suppress the grain growth in the doped sample. Hence, the doped sample has more space for active sites which is favourable for the electrochemical process.

Table 23 - Parameters obtained from the Rietveld refinements for Fe,Cr:$ZnCo_2O_4$

Sample/Parameter	**Fe, Cr: $ZnCo_2O_4$**
Crystal system /Space group	$Fd\bar{3}m$
Cell parameter (Å)	a= b=c=8.0945
Cell Volume ($Å^3$)	530.359
Co-Ordinates (x,y,z)	Zn (0.125, 0.125, 0.125) Co (0.625, 0.625, 0.625) O (0.377, 0.377, 0.377) Fe (0.007, 0.077, 0.077) Cr (1.570, 1.570, 1.570)
Occupancy	Zn 0.612; Fe 0.211; Cr 0.216; Co 0.953; O 0.993
Density (gm cm^{-3})	7.310
α, β, γ	90°
W_R	4.863
GOF	1.60

Table 24 - Parameters calculated from the X-ray diffractogram of Fe,Cr:$ZnCo_2O_4$

Sample / Parameter	**2θ (311) (º)**	**β (311) (º)**	**d (311) (Å)**	**Crystallite size (nm)**	**Strain (ε)**	**Dislocation density (x10^{15}) /cm^3**
Fe, Cr: $ZnCo_2O_4$	36.71	0.28	2.44	27.63	0.22	1.30

8.3. Raman Analysis of Fe,Cr:$ZnCo_2O_4$

Raman spectra of Fe, Cr: $ZnCo_2O_4$ is shown in Figure 60. The corresponding Raman peaks for doped sample are given in Table 25. Compared to pristine sample, the Raman peaks observed at 198 (F_{2g}(3)), 472 (E_g), 527 (F_{2g}(2)) , 619 (F_{2g}(1)) and 691 (A_{1g}) cm^{-1} are

shifted towards the higher wavenumber (longer frequency) indicating that the bond lengths have become shorter compared to the atomic positions in the undoped $ZnCo_2O_4$. Two peaks at wavenumber 487 and 535 cm^{-1} are additionally seen which can be attributed to the chromium occupying half of the octahedral interspaces and iron occupying the one eighth of the tetrahedral interspaces **(Kaliwoda et al., 2021; Lazarević et al., 2012)** which can be visualized in the unit cell of the Fe, Cr doped $ZnCo_2O_4$ derived from the result of Rietveld analysis of XRD using Vesta software.

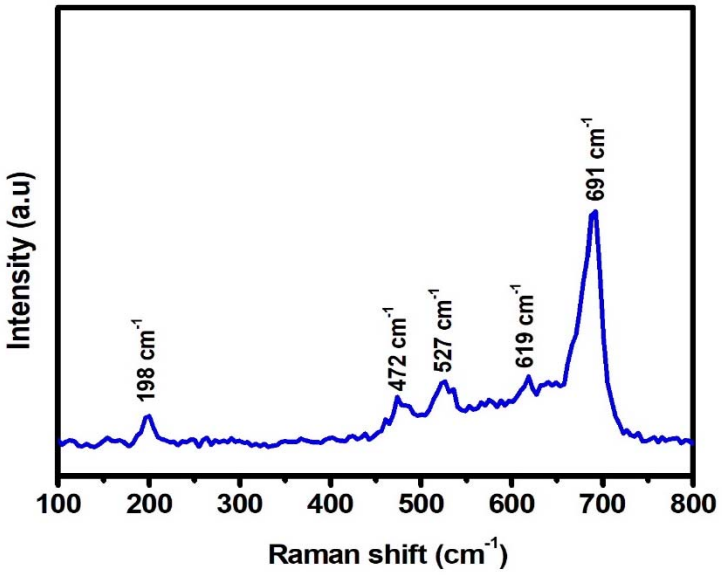

Figure 60 - Raman spectra of Fe,Cr:$ZnCo_2O_4$

Table 25 - Assignments of Raman peaks of Fe,Cr:$ZnCo_2O_4$

Raman Band (cm^{-1})	Symmetry species	Assignment
198	F_{2g} (3)	δ(Zn-O)
472	E_g	ν (Co-O) + ν (Zn-O)
527	F_{2g} (2)	ν(Co-O)
619	F_{2g} (1)	ν(Co-O)
691	A_{1g}	ν(Co-O)

8.4. FESEM Analysis of Fe,Cr:$ZnCo_2O_4$

Morphological features of Fe, Cr: $ZnCo_2O_4$ are observed from FESEM micrographs and are shown in Figure 61. These micrographs exhibit heterogeneous grain distribution. The magnification of x 96300 in 5µm scale clearly shows the octahedral morphology. When compared to pristine material, the smaller particles are aggregated on the surface of the octahedral shaped particles. The particle size of the Fe and Cr doped $ZnCo_2O_4$ sample exceeds > 500nm.

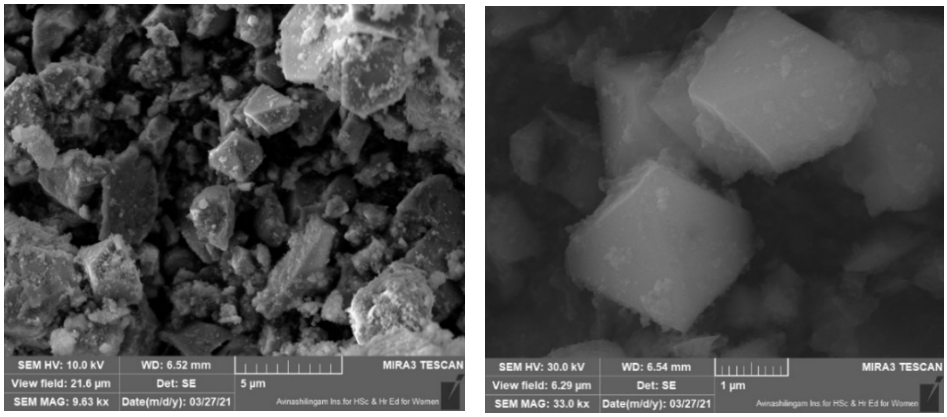

Figure 61 - FESEM micrographs of Fe,Cr:$ZnCo_2O_4$

8.5. Elemental Analysis of Fe,Cr:$ZnCo_2O_4$

The EDAX spectrum of the Fe, Cr: $ZnCo_2O_4$ material is shown in Figure 62. In EDX spectra, the intense peaks at 0.52 keV and 0.77 keV and corresponds to the Kα lines O and Co respectively. A carbon peak at 0.28 keV has come up from the tape used for analysis. The peak exhibits at 1.01 keV and 6.92 keV are the Lα lines of Zn and Co elements. In addition to Zn, Co and O, the peak at 6.40 keV and 5.41 keV are attributed to the Kα lines of Fe and Cr elements. There are other minor peaks emerging due to impurities 1.76 (Si), 2.15 (S), 2.63 (Cl), 3.33(K), 3.69(Ca) 5.98 (Mn) and 7.47 (Ni) are also seen that have got incorporated in the sample as the parental chemicals of chlorides contained it. Other than Mn and Ni, all the other elements are very feable for contributing to any of the electrochemical performance. The atomic weight percentages of the elements are given in Table 26.

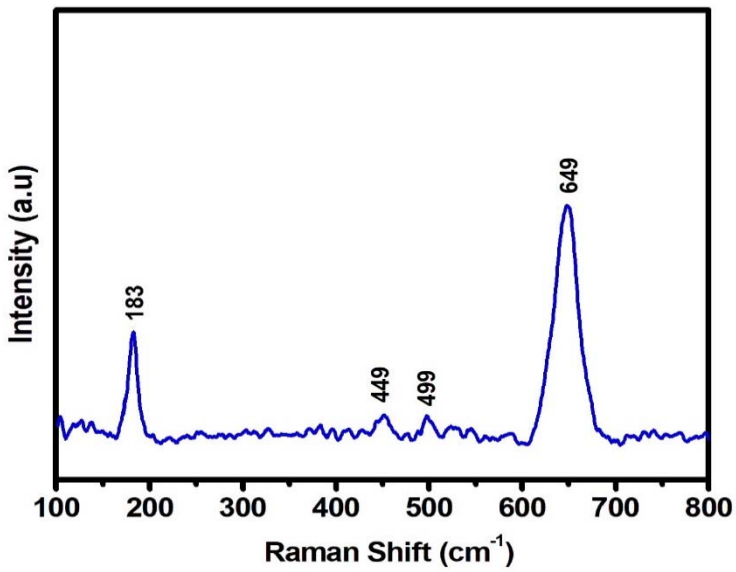

Figure 62 - EDX spectrum of Fe,Cr:ZnCo2O4

Table 26 - Elemental composition of Fe,Cr:$ZnCo_2O_4$

Elements	Atomic weight percentage
Zn	3.59
Co	40.47
O	39.71
Fe	5.41
Cr	10.82

8.6. Electrochemical properties of Fe, Cr: $ZnCo_2O_4$

8.6.1. Cyclic Voltammetry analysis of Fe,Cr:$ZnCo_2O_4$

The cyclic voltammetry analysis of Fe and Cr doped $ZnCo_2O_4$ is given in Figure 63. For this investigation, the coated electroactive material on current collector (Cu foil) is cut into required dimension of 1x1 cm^2 and analyzed with Pt counter as counter electrode and Ag/AgCl as reference electrode. The Fe and Cr doped Zinc cobaltite sample shows the potential window of 0 to 0.5 V. The potential window remains the same as in the pristine structure even for the doped sample. The CV graph shows entirely deviated rectangular shape indicating that the charge storage mechanism of doped material arises from the

pseudocapacitive behaviour. When looking into the CV analysis, it is clear that the dopants have enhanced the electrochemical activity of the pristine material which is reflected by increasing the current and area under the CV curve profiles.

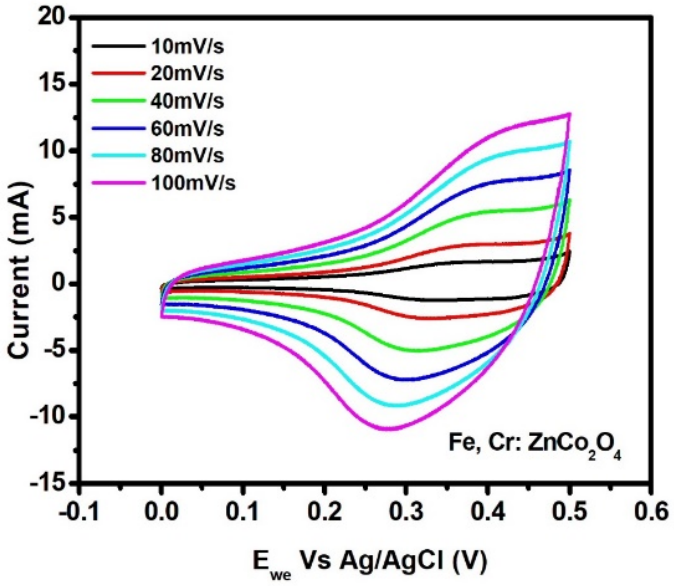

Figure 63 - Cyclic voltammogram of Fe,Cr:$ZnCo_2O_4$

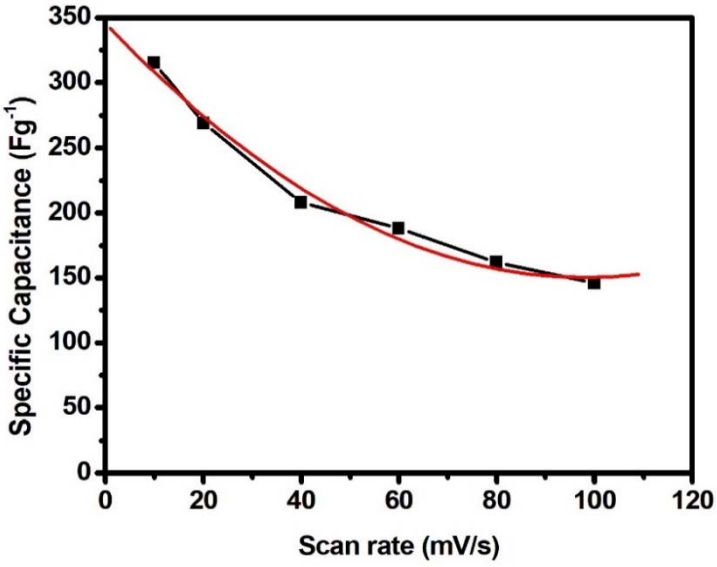

Figure 64 - Plot of scan rate vs specific capacitance of Fe,Cr:$ZnCo_2O_4$

The specific capacitance values for Fe and Cr doped $ZnCo_2O_4$ are 315, 269, 208, 188, 162 and 146 Fg^{-1} at the scan rate of 10 mV/s, 20 mV/s, 40 mV/s, 60 mV/s, 80 mV/s and 100 mV/s. The changes of specific capacitance with respect to scan rate is shown in

Figure 64. The specific capacitance value decreases with increase of scan rates due to the fact that at low scan rates, electrolyte ions have enough time to migrate into the electrode material and probably react with all possible electro-active species, whereas at fast scan rates, only surface-active sites are involved in the electrochemical reaction. The fitting with polynomial resulted in a quadratic equation $y= 0.02034x^2-3.98812x+345.81$. Unlike a third order fit in the pristine the fit has reduced one order indicating the dependency of a factor is curtailed in the doped sample compared to the pure $ZnCo_2O_4$ presented in the previous Chapter. The quadratic solution will result in a complex number. But, looking at the real component, the capacitance at optimal scan rate would be 99.52 which is an indication of high stability of the material to yield better specific capacitance.

8.6.2. Galvanostatic Charge-Discharge analysis of Fe, Cr: $ZnCo_2O_4$

GCD analysis has been carried out in the potential window of 0V-0.5 V shown in Figure 65. It shows the non-linear triangular shaped GCD curves indicating the existence of pseudocapacitive behaviour, which agrees with the results found in CV. From the GCD curves, the maximum specific capacitance value of 320 Fg^{-1} is reached at a current density of 1 Ag^{-1} for Fe, Cr: $ZnCo_2O_4$ sample. It is compared with already reported articles of $ZnCo_2O_4$ which are discussed in previous Chapter 7.

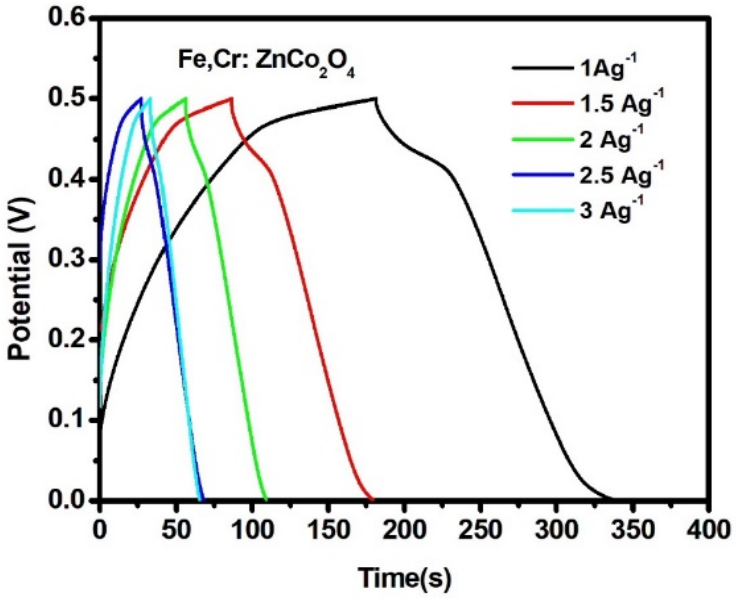

Figure 65 - Galvanostatic Charge-Discharge curves of Fe,Cr:$ZnCo_2O_4$

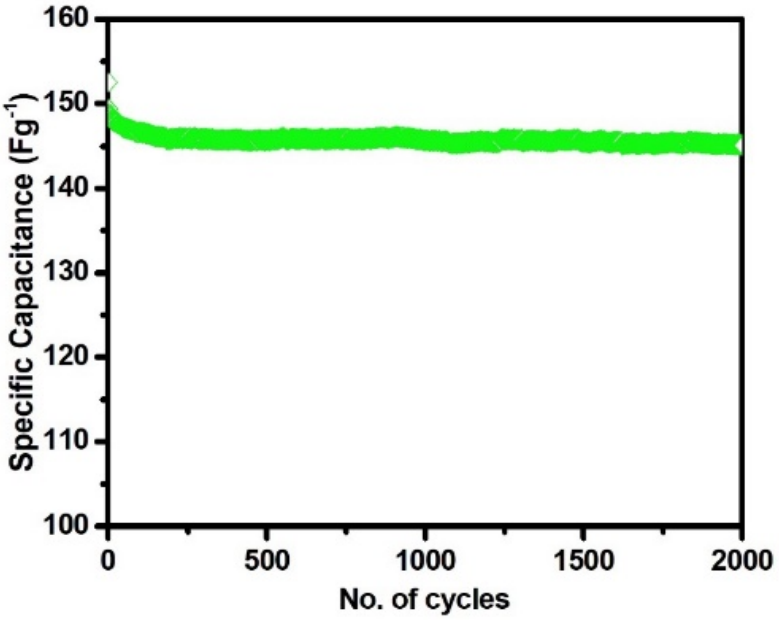

Figure 66 - Cyclic stability of Fe,Cr:$ZnCo_2O_4$

The value of the specific capacitance for Fe and Cr doped sample is higher than the pristine sample which may be due to the effect of doping into host elements. The cycling stability of Fe, Cr: $ZnCo_2O_4$, is tested over a period of 2000 cycles and displayed in Figure 66. The Fe, Cr: $ZnCo_2O_4$ has capacitance retention of 94% at 5 Ag^{-1} for 2000 cycles indicating better electrochemical stability than the pure $ZnCo_2O_4$ due to the addition of dopants. When compared to previously reported literature **(Rajesh et al., 2016; Raut & Sankapal, 2017; Xu et al., 2017),** Fe, Cr: $ZnCo_2O_4$ has an excellent cycling stability than reported pristine $ZnCo_2O_4$ which concludes that the dopants have effectively increased the electrochemical performance of the pristine material.

8.6.3. Electrochemical Impedance analysis of Fe, Cr: $ZnCo_2O_4$

Electrochemical impedance analysis has been performed for Fe, Cr: $ZnCo_2O_4$ using 1M KOH as an electrolyte to estimate the electrochemical properties. From Figure 67, it reveals that the Fe, Cr: $ZnCo_2O_4$ shows a semi-circle in frequency region followed by another partial semicircle. The obtained Nyquist plots are fitted with EC- lab software, and the equivalent circuit is similar to that of pure Zinc cobaltite.

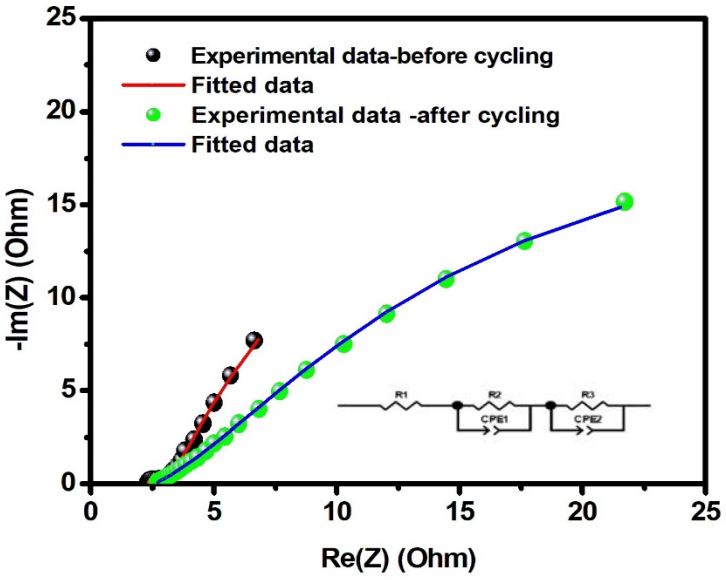

Figure 67 - Electrochemical impedance spectra of Fe,Cr:$ZnCo_2O_4$

Table 27 - Fitted parameters of electrochemical impedance spectra of Fe,Cr:$ZnCo_2O_4$

Parameters	Fe, Cr: $ZnCo_2O_4$	
	Before Cycling	After Cycling
$R_1(\Omega)$	2.17	2.62
$R_2(\Omega)$	0.88	20.77
CPE 1	$8.33x10^{-3}$	$7.22x10^{-3}$
n1	0.54	0.41
CPE 2	0.15	0.07
n2	0.76	0.79
$R_3(\Omega)$	124.3	36.82

Before cycling, the value of solution resistance (R_1) and charge transfer resistance (R_2) for Fe, Cr: $ZnCo_2O_4$ are 2.17 Ω and 0.88 Ω. The charge transfer resistance before cycling in this case is too small. After cycling, the charge transfer resistance is high which indicates the formation of electrode - electrolyte interface. However, Fe and Cr doped sample exhibits lower charge transfer resistance post cycling compared to pure $ZnCo_2O_4$.

The specific capacitance of doped sample is 320 Fg^{-1} compared to the pure which was 266 Fg^{-1}. The fitted parameters calculated from the equivalent circuit are given in Table 27. Overall, the electrochemical characterizations (CV, GCD and EIS) conclude that the electrochemical performance is better for Fe, Cr: $ZnCo_2O_4$ when compared with pristine which is due to the addition of dopants into pristine material.

8.7. Summary

The Fe and Cr doped $ZnCo_2O_4$ has been prepared by sol-gel method and analysed. Structural analyses through XRD and subsequent Rietveld process reveal the cubic spinel structure. The positional coordinates are evaluated with the best fit and found that the Co and O has not been disturbed and the sharing of Zn site by Fe and Cr has brought in several vacancies possible with 28% vacancy in the unit cell. The Raman analysis also appended the change in environment in the unit cell with two newer peaks at wavenumbers 487 and 535 cm^{-1} that are attributed to chromium occupying half of the octahedral interspaces and iron occupying the one eighth of the tetrahedral interspaces. The electrochemical performance of the Fe and Cr doped $ZnCo_2O_4$ has been analysed with 1M KOH aqueous electrolyte solution, and it shows the specific capacitance of 320 Fg^{-1} at the current density of 1 Ag^{-1} and capacitance retention of 94 % over 2000 cycles and is higher than the pristine sample. In conclusion, the dopants such as Fe and Cr incorporated in $ZnCo_2O_4$ has enhanced the electrochemical performance of the pristine sample. Hence, Fe and Cr doped $ZnCo_2O_4$ has been employed as the promising electrode for supercapacitor applications.